Proceedings of the Thirty-second (2022) International Ocean and Polar Engineering Conference **www.isope.org**
Shanghai, China, June 5–10, 2022

ISBN 978-1-880653-81-4; ISSN 1098-6189

CFD Study of Trimaran Seakeeping Performance with Various Wave-lengths

Yabo Wei[1], Qingjie Meng[2], Decheng Wan[1]*

[1] Computational Marine Hydrodynamics Lab (CMHL), School of Naval Architecture, Ocean and Civil Engineering, Shanghai Jiao Tong University, Shanghai, China
[2] Wuhan Second Ship Design and Research Institute, Wuhan, China
[*]Corresponding author

ABSTRACT

The trimaran has received increasing attention for its excellent resistance and maneuverability. Based on the in-house ship hydrodynamics CFD solver naoe-FOAM-SJTU, the seakeeping performance of trimaran in regular waves when Fr=0.18 is simulated. Firstly, grid convergence verification is carried out. Then, the seakeeping performance of the trimaran on different wavelengths is carried out by numerical methods, and the calculation results including heave and pitch motion of trimaran are compared with the experimental results. Studies have shown that the amplitudes of heave and pitch motion get larger with the increase of wavelength on the whole. The numerically simulated results agreed very well with the experimental data which the experiment work is in progress and the report is not officially published. Their agreement shows that the naoe-FOAM-SJTU solver can be used to predict the seakeeping performance of the trimaran and provide data support for the design process of the trimaran.

KEY WORDS: Trimaran; CFD; regular wave; heave; pitch

INTRODUCTION

Trimaran has become more and more popular due to its excellent maneuverability and resistance in recent years. It consists of a main hull and two side-hulls, which leads to a larger deck area. With the development of computer technology, Computer Fluid Dynamics (CFD) based on viscous theory has been widely applied in hydrodynamic problems of trimarans. Compared to traditional mono-hull, the hydrodynamic performance of trimaran in waves is more complicated. Besides, accurately predicting the motion response of trimaran in waves is a prerequisite for trimaran's design. However, the nonlinearity between main hull and side-hulls is high so that the potential flow theory is not suitable to study the seakeeping performance of trimaran. Therefore, the computer fluid dynamics (CFD) based on viscous theory is used to study the seakeeping performance of trimaran in this paper.

Unlike navigating in calm water, trimaran navigating in waves will dissipate more energy. This additional energy consumption is called added resistance (Arribas, 2020). Consequently, when studying the seakeeping performance of trimaran, the added resistance in waves will also be considered. Gong, Yan and Ma (2020) apply a hybrid method to study the trimaran's added resistance and seakeeping performance in oblique waves. The results show that the wave steepness and wave incident will affect the trimaran's added resistance and seakeeping performance in waves. Gong, Li and Fu (2021) study the trimaran's seakeeping performance in waves of various headings at various speeds and find that the sailing speed has larger effect on added resistance than motion. Besides, some scholars try to improve trimaran's seakeeping performance by changing the layout of side-hulls (Wang, Ma and Duan, 2018; Nazemian, Ghadimi P, 2021; Wang, Duan, 2021; Ghadimi, Nazemian and Ghadimi, 2019). The results show that the trimaran will gain suitable dynamics and reduce the added resistance by reasonably setting the side-hulls' arrangement.

In addition, T-foil (Moret, Perez and Tejedor, 1993) is an effective component in reducing the trimaran's pitch motion and shows some good results by applying it on trimarans. Deng, Huang and Zhou (2014) compared the pitch and heave motion of trimaran with and without T-foil, and they found that the T-foil can effectively mitigate the motions of trimaran in waves. Jiang, Bai and Liu (2022) proposed a hybrid control strategy that has a better result in reducing the motion response of trimaran to control the T-foil which can adjust the maximum flap angel according to the trimaran's motion response. In order to further improve trimaran's seakeeping performance, stern-flap and T-foil are often combined to be installed. Zheng, Liu and Yang (2021) selected the T-foil and stern-flap to study the influence of installation positions on seakeeping performance, and verify whether the appendages' installation positions are reasonable and effective to improve the seakeeping performance of trimaran in waves. Zeng, Song and Zheng (2019) designed an active controller of the appendages based on T-foil and flap, and the experiment results show that the controller has a good effect on trimaran's vertical stabilization.

To sum up, trimaran has gradually attracted more and more scholars' attention due to its excellent seakeeping performance. However, compared with the research on resistance of trimaran, there are relatively few studies on the seakeeping performance of trimaran. This paper studies the characteristics of trimaran seakeeping performance with various wave-lengths when Fr=0.18 based on our in-house solver naoe-FOAM-SJTU. Compared with the experimental results, it shows that the naoe-FOAM-SJTU solver can be used to predict the seakeeping performance of the trimaran and provide reference for the design process of the trimaran.

NUMERICAL METHOD

Governing equations

In order to predict the trimaran's motions, the flow is assumed to be incompressible, unsteady and viscous. The governing equation is Reynolds averaged Navier-Stokes equation which is presented as follows.

$$\nabla \cdot \mathrm{U} = 0 \tag{1}$$

$$\begin{aligned}&\frac{\partial \rho \mathrm{U}}{\partial t} + \nabla \cdot (\rho(\mathrm{U} - \mathrm{U}_g)\mathrm{U} \\ &= -\nabla p_d - g \cdot x \nabla \rho + \nabla \cdot (\mu_{eff} \nabla \mathrm{U}) \\ &\quad + (\nabla \mathrm{U}) \cdot \nabla \mu_{eff} + f_\sigma + f_s\end{aligned} \tag{2}$$

where U is the velocity, U_g is the is the velocity of the computational grid, p_d is the dynamic pressure, g is the gravitational acceleration, μ_{eff} is the coefficient of dynamic viscosity, f_σ is the surface tension, fs is the source term applied in the relaxation zone.

Turbulence model

In this this work, the SST k-ω turbulence model is chosen to solve the trimaran's motion in waves. The concrete equations about the SST k-ω turbulence model can be found in (Menter, 1992).

Free surface modeling

In order to accurately capture the free surface when trimaran sailing in marine, this work use the volume of fluid (VOF) method to control the numerical spread. The equations can be expressed as:

$$\frac{\partial \alpha}{\partial \mathrm{t}} + \nabla \cdot [(\mathrm{U} - \mathrm{U}_g)\alpha] + \nabla \cdot [\mathrm{U}_r(1-\alpha)\alpha] = 0 \tag{3}$$

where ρ is the fluid density, α is the volume fraction and $0<\alpha<1$. The volume fraction α can be expressed as:

$$\alpha = \begin{cases} 0 & \text{air} \\ 1 & \text{water} \end{cases} \tag{4}$$

At the same time, the fluid density ρ and the coefficient of dynamic viscosity μ_{eff} can also be expressed by α.

$$\rho = \alpha \rho_l + (1-\alpha)\rho_g \tag{5}$$

$$\mu = \alpha \mu_l + (1-\alpha)\mu_g \tag{6}$$

where the subscripts l and g represent respectively fluid and gas.

The surface tension f_σ in Eq. 2 can be defined as.

$$f_\sigma = \sigma \kappa \nabla \alpha \tag{7}$$

where σ is the surface stress tensor and its value is 0.07 kg/s^2 in this study, κ is the curvature of the interface, and κ satisfies the equation presented as.

$$\kappa = -\nabla \cdot \mathrm{n} = -\frac{\Sigma_f \mathrm{S}_f \cdot \mathrm{n}_f}{V_i} \tag{8}$$

where V_i is the unit volume, the subscript f represents the calculated value of the element surface, which represents the sum of the surface calculated values of each grid element, S_f indicates the normal vector to the element surface. n_f represents the unit normal vector of the interface, given by.

$$n_f = \frac{(\nabla \alpha)_f}{\left|(\nabla \alpha)_f + \delta\right|} \tag{9}$$

where δ is the stability factor.

$$\delta = \frac{1 \times 10^{-8}}{\left(\frac{\sum_{i=1}^{N} V_i}{N}\right)^{1/3}} \tag{10}$$

where N is the total number of grid cells.

NUMERICAL COMPUTATION

Geometry model

The geometry model of the trimaran is shown in Fig. 1, and the figure trimaran's principal dimensions in model scale are provided in Table 1.

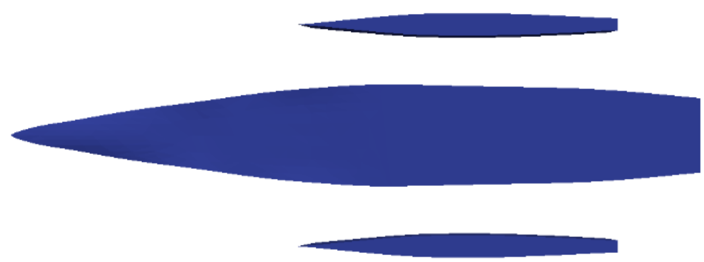

Fig. 1. Geometry model of trimaran

Table 1. Main particulars of trimaran

Particulars	Symbols and units	Value
Length between perpendiculars	L_{pp} (m)	5.4
Total width	B (m)	0.65
Draft	T (m)	0.18
Depth	D (m)	0.46
Displacement	∇ (m^3)	0.295
Wet surface area	S_w (m^2)	3.38

Test conditions and numerical settings

The conditions in this work to evaluate the seakeeping performance of trimaran are shown in Table 2 below.

Table 2. Test conditions

Conditions	Symbols and units	Value
Velocity	U (m/s)	1.3094
Froude number	Fr	0.18
Wave-length	λ/L_{wl}	0.9、1.0、1.1、1.2、1.3、1.4、1.5、1.6、1.7、1.8
Wave height	H_s (m)	0.12
Wave direction angle	X (deg)	0

Since the trimaran is symmetrical about the mid-longitudinal section, the numerical calculation domain used in this work is the half-vessel calculation domain, which can greatly reduce the calculation cost and time. The pretreatment tools blockMesh and snappyHexMesh in OpenFOAM are used to generate grid, which the blockMesh is used to generate background grid and the snappyHexMesh is used to generate grid around the hull, local refinement, and add boundary layers. The computational domain size and grid information are shown respectively in Fig. 2 and Fig. 3, and the concrete boundary conditions are shown in Table 3. The boundary conditions are shown in Fig. 2.

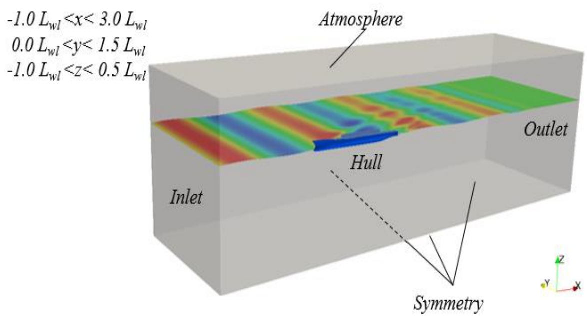

Fig. 2. Computational domain

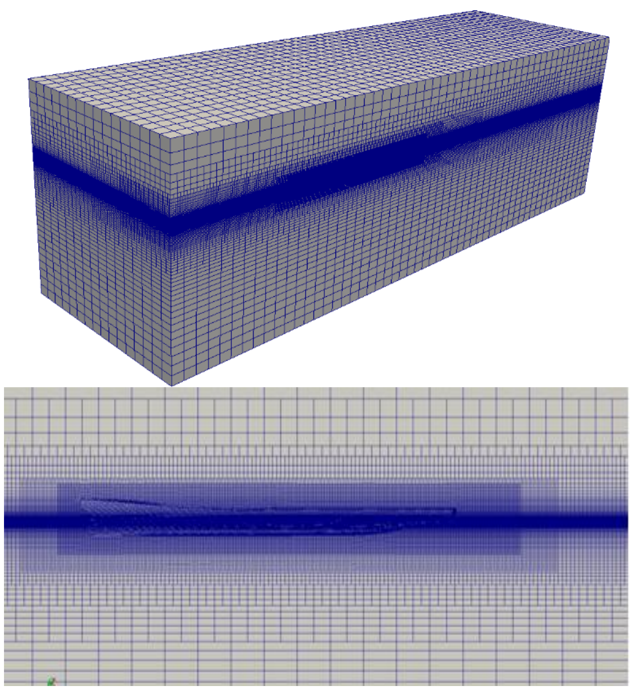

Fig. 3. Mesh distribution

Table 3. Boundary conditions

Boundry	Boundary conditions
Inlet	Velocity inlet
Atmosphere	Non-slip condition
Symmetry	Non-slip condition
Hull	Non-slip wall condition
Outlet	Pressure outlet

Grid convergence verification

According to the above settings, grid convergence verification is carried out on heave, pitch motion of trimaran in the regular wave of heading waves when Fr=0.18. The regular wave with (λ/L_{pp}) =1 is used for the grid uncertainty test. Three sets of grids with different densities are used as shown in Fig. 4, and the size of the background grids of adjacent sets of grids in the direction of each coordinate axis is in a $\sqrt{2}$ relationship. The number of the three sets of grids is shown in Table 4.

Table 4. Grid number settings of three sets

Three sets of grid	Background grid number	Grid density
S3	38×8×84	948895
S2	54×12×120	2799456
S1	76×16×168	7172111

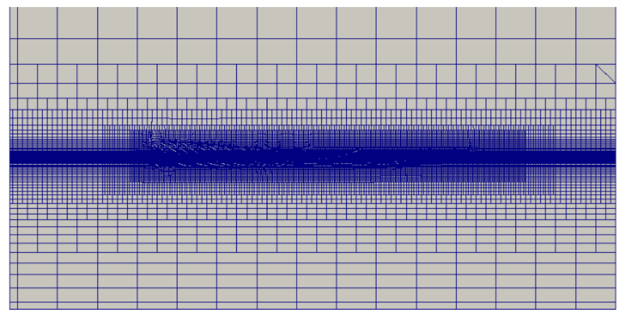

(a) Coarse (S3)

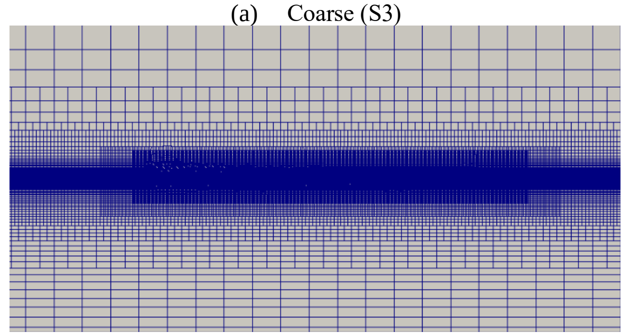

(b) Medium (S2)

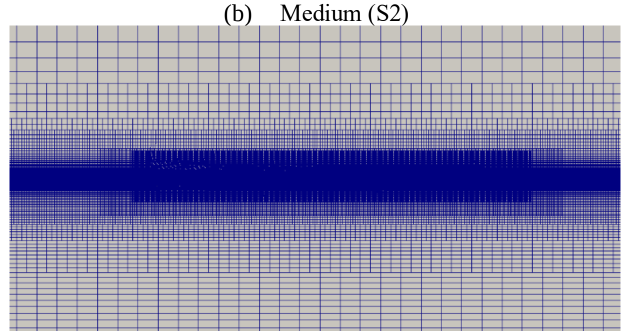

(c) Fine (S1)

Fig. 4. Computational meshes for grid uncertainty analysis

In order to better measure the motion response of the trimaran in the regular wave, the response of the trimaran in the regular wave is subjected to dimensionless processing, and the processed frequency response function is:

$$H_{z(w)} = \frac{z_a}{\zeta_a} \tag{11}$$

$$H_{z(\theta)} = \frac{\theta_a}{(k\zeta_a)} \tag{12}$$

where z_a is the amplitude of heave motion, θ_a is the amplitude of pitch motion, k is the wavenumber, ζ_a is the wave amplitude of regular wave.

The experiment results when λ/L_{pp} =1 is shown in Table 5. Finally, after the wave field is fully evolved and the typical physical quantities in the flow field show stable cyclical changes, counting the typical physical quantities in one period to gain the heave and pitch motion amplitude which are shown in Table 6. The time history of wave elevation is shown in Fig. 5. According to Fig. 5, the pitch and heave motion amplitudes from three sets of data are so close to each other that their differences are almost invisible. At the same time, combined with Table 5 and Table 6, it is found that the two physical quantities converge uniformly. Consequently, a 'convergent' solution can be obtained by doing a series of encryptions on this basis. Therefore, the grid layout is relatively reasonable. Considering comprehensively the computational accuracy and efficiency, the medium grid will be used to study the seakeeping performance with various wave-lengths.

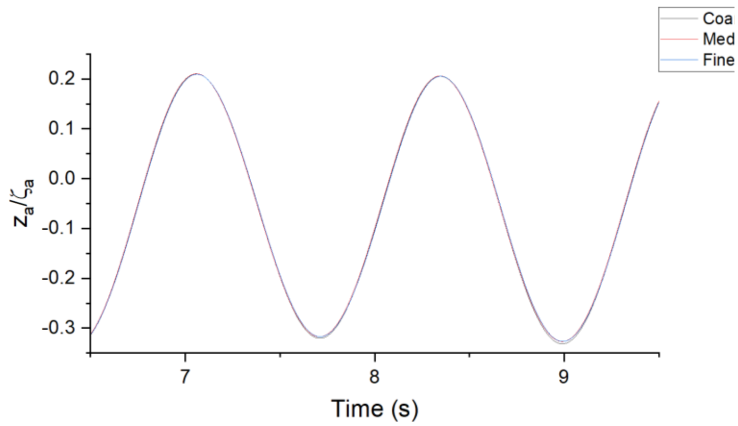

(a) Heave motion

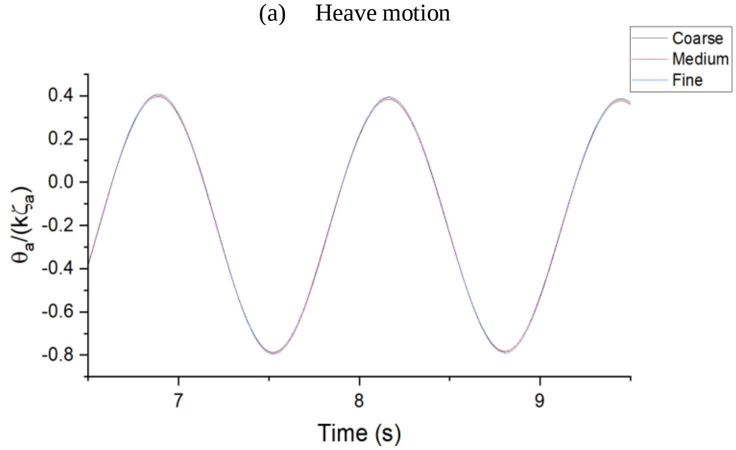

(b) Pitch motion

Fig. 6. Time history of wave elevation

Table 5. Experiment results when λ/L_{pp}=1

	EFD
Heave motion(z_a/ζ_a)	0.5088
Pitch motion($\theta_a/(k\zeta_a)$)	0.5640

Table 6. Uncertainty analysis for trimaran in regular wave when λ/L_{pp}=1

Grid number	Heave motion(z_a/ζ_a)	Pitch motion ($\theta_a/(k\zeta_a)$)	Error(Heave motion)	Error(Pitch motion)
S3	0.5439	0.5823	6.90%	3.24%
S2	0.5278	0.5791	3.73%	2.68%
S1	0.5313	0.5813	4.42%	3.07%

Comparison of CFD and EFD

Based on the medium grid, the heave and pitch motion of the trimaran are compared with the experimental values which are shown in Fig. 5. The results in Fig. 6 show that the amplitudes of heave and pitch motion get larger with the increase of wavelength on the whole. The maximum error about heave and pitch motion of trimaran are 4.33% and 3.60%, respectively. The numerically simulated results agreed very well with the experimental data which the experiment work is in progress and the report is not officially published. Their agreement shows that the naoe-FOAM-SJTU solver can be used to predict the seakeeping performance of the trimaran and provide data support for the design process of the trimaran. When the wave-length gets larger from $0.9L_{wl}$ to $1.6L_{wl}$, the motion response of the trimaran increases substantially. However, the motion response of the trimaran increases gradually when the wave-length increases from $1.6L_{wl}$ to $1.8L_{wl}$. Fig. 7 shows the free surface wave shape with various wave-lengths.

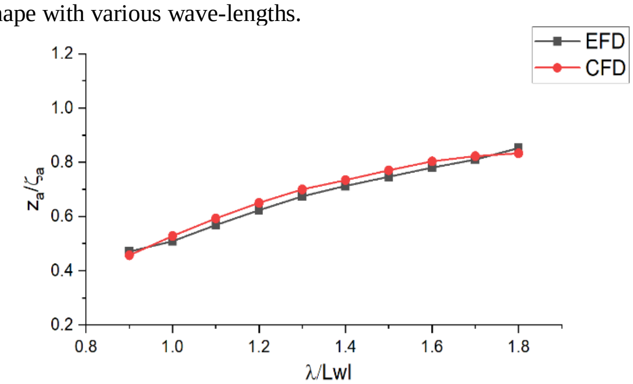

(a) Heave motion

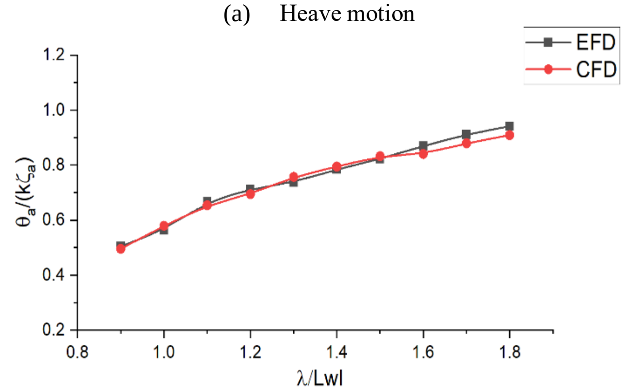

(b) Pitch motion

Fig. 6. Computational meshes for grid uncertainty analysis

Fig. 7 shows the free surface wave with various wave-lengths when Fr=0.18. Compared with the free surface wave shape with various wave-lengths. According to Fig. 6, when other conditions are the same, the V-shaped opening of the hull wave increases with the increase of the wave-length. When the wave-length gets larger, the flow field changes is relatively flat, which can explains the reason why the motion response changes from fast to relatively slow. In addition, with the increase of the wave-length in the regular wave, after the wave-making generated by trimaran sailing in the sea and the regular wave are superimposed, the influence on the flow field waveform becomes more and more obvious, especially in the Fig. 7(j) which the wave-length is λ=1.8Lwl. The outward diffusion range of the wave-making is small, so the wave-making pair has a large disturbance to the flow field around the hull. However, in the region of λ=0.9Lwl in Fig. 7(a), the equivalent height of wave-making at the bow and stern is larger, and the range of the outward diffusion of the waveform is larger. At the same time, it can also be observed that the influence of wave making around the hull is greater than that of other working conditions in Fig. 7(j).

Fig. 8 shows the wave elevations in one wave encounter period of trimaran when Fr=0.18. It's found that due to the strong nonlinearity between the main hull and the side-hulls, the potential flow theory is not suitable to study the motion of trimaran in regular waves. During the entire encounter period, since the phase of the incident wave keeps changing, that is to say, the positions of the crests and troughs keep changing. As a result, the wave-making interference between the main hull and the side-hulls keeps changing, and the favorable and unfavorable interference changes periodically. Thus, there is an obvious difference in the wave surface between the outside of the side-hulls and the main hull and the side-hulls, indicating that the pressure distribution on both side-hulls is no longer symmetrical. Overall, the wave surface changes between the main hull and the side-hulls are more severe than those outside the side-hulls over the entire encounter period. When the wave crest is at the bow position, the bow trim phenomenon can be seen from Fig. 8(a). When the wave crest is at the middle of the trimaran, the sagging moment to hogging moment can be seen from Fig. 8(b) and Fig. 8(c). Similarly, the stern trim can be seen in Fig. 8(d) when the wave crest at the stern position. However, the motion response is not severe, because the velocity of trimaran is not very high.

CONCLUSION

Based on our in-house viscous flow solver, the numerical simulation of the seakeeping performance of trimaran at different wave-lengths is carried out in this paper. The calculation results are compared with the experimental results. The concrete conclusions are presented as follows:

(a) Through the numerical simulation based on our in-house solver naoe-FOAM-SJTU, the heave and pitch motion at various wave-lengths are compared with experimental results. It's found that the numerically simulated results agreed very well with the experimental data which the experiment work is in progress and the report is not officially published. Their agreement shows that the naoe-FOAM-SJTU solver can be used to predict the seakeeping performance of the trimaran and provide data support for the design process of the trimaran.
(b) The amplitudes of heave and pitch motion get larger with the increase of wavelength on the whole. When the wave-length gets larger, the flow field changes is relatively flat. In addition, with the increase of the wave-length in the regular wave, after the wave-making generated by trimaran sailing in the sea and the regular wave are superimposed, the influence on the flow field waveform becomes more and more obvious.

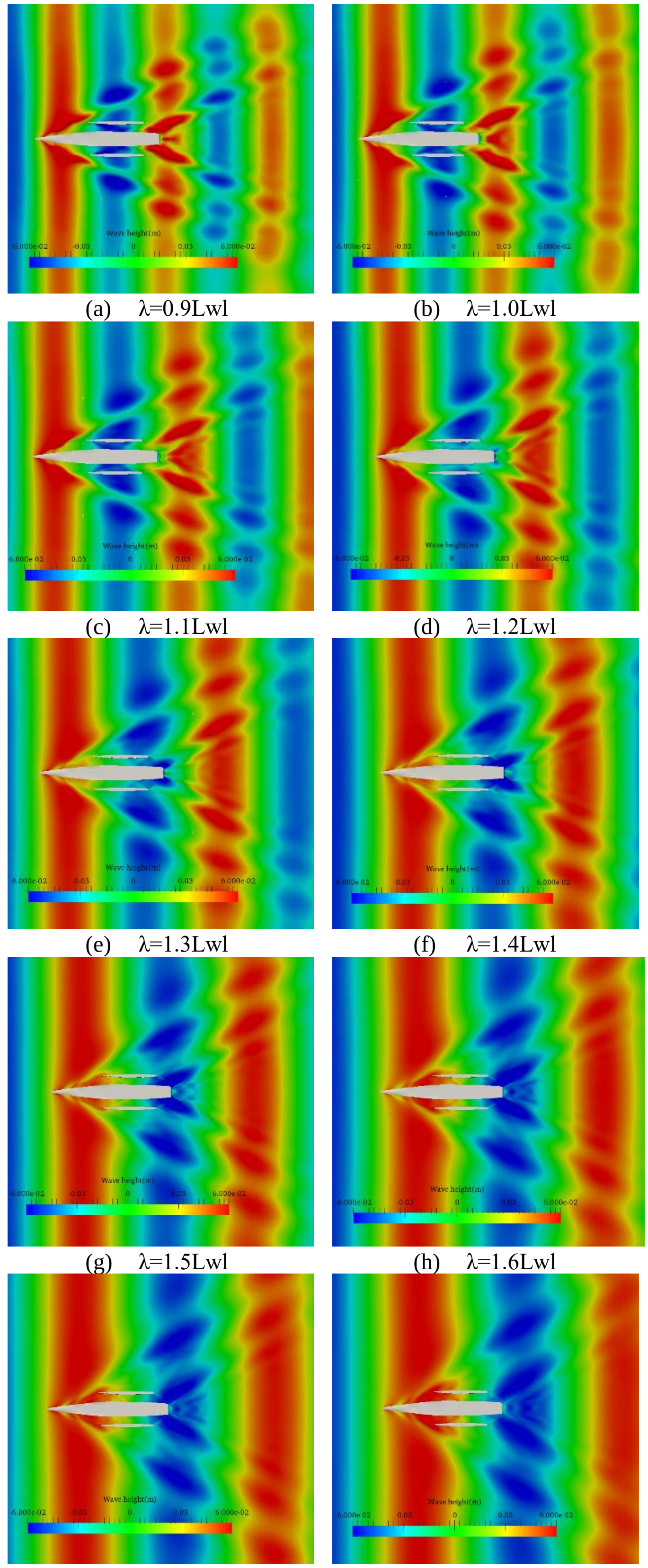

Fig. 7. Free surface wave with various wave-lengths

This paper only studies the trimaran seakeeping performance with various wave-lengths, and does not pay attention to the added resistance of trimaran in waves. The heave and pitch motion in the range (wave length)/(ship length)=0.4~0.8 is not simulated because of the calculation time and computing resources. In the future, the author will focus on both seakeeping performance and added resistance in waves to explore the influence of wave-length in the range (wave length)/(ship length)=0.4~0.8.

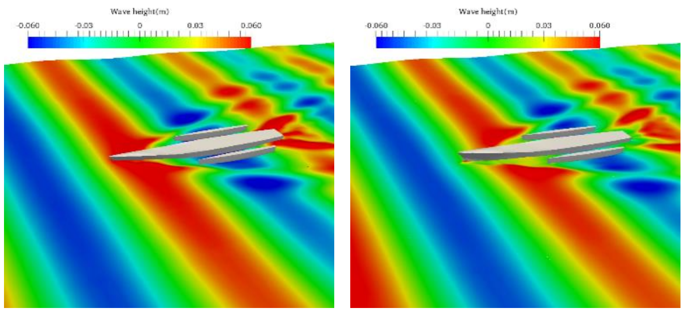

(a) t=nT$_e$ (b) t=(n+1/4)T$_e$

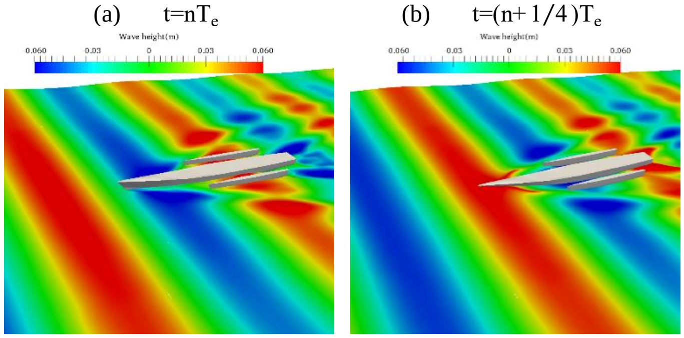

(c) t=(n+1/2)T$_e$ (d) t=(n+3/4)T$_e$

(e)

Fig. 8. Wave elevations in one wave encounter period of trimaran

ACKNOWLEDGEMENTS

This work was supported by the National Natural Science Foundation of China (51879159, 52131102), and the National Key Research and Development Program of China (2019YFB1704200), to which the authors are most grateful.

REFERENCES

Arribas F P. Some methods to obtain the added resistance of a ship advancing in waves [J]. *Ocean Engineering*, 2007, 34(7): 946-955.

Deng R, Huang D, Zhou G. Research on the Influence of T-foil on the Hydrodynamic Performance of Trimaran[C]//*The Twenty-fourth International Ocean and Polar Engineering Conference*. OnePetro, 2014.

Ghadimi P, Nazemian A, Ghadimi A. Numerical scrutiny of the influence of side hulls arrangement on the motion of a Trimaran vessel in regular waves through CFD analysis [J]. *Journal of the Brazilian Society of Mechanical Sciences and Engineering*, 2019, 41(1): 1-10.

Gong J, Yan S, Ma Q, et al. Added resistance and seakeeping performance of trimarans in oblique waves [J]. *Ocean Engineering*, 2020, 216: 107721.

Gong J, Li Y, Fu Z, et al. Study on the characteristics of trimaran seakeeping performance at various speeds [J]. *Journal of the Brazilian Society of Mechanical Sciences and Engineering*, 2021, 43(4): 1-16.

Jiang Y, Bai J, Liu S, et al. Experimental investigation of T-foil hybrid control strategy for ship motion reduction in head seas [J]. *Ocean Engineering*, 2022, 243: 110251.

Menter F R. Improved two-equation k-turbulence models for aerodynamic flows [J]. *NASA Technical Memorandum*, 1992, 103975(1_): 3t.

Moret J A, Perez de Lucas A, Tejedor J L. Fast ferry Mestral: A reliable answer in fast ferry design [J]. 1993.

Nazemian A, Ghadimi P. Multi-objective optimization of trimaran sidehull arrangement via surrogate-based approach for reducing resistance and improving the seakeeping performance [J]. *Proceedings of the institution of mechanical engineers, part M: journal of engineering for the maritime environment*, 2021, 235(4): 944-956.

Wang S M, Duan W Y. Study on the multi-objective optimization method of trimaran outrigger layout [J]. *Ships and Offshore Structures*, 2021: 1-7.

Wang S M, Ma S, Duan W Y. Seakeeping optimization of trimaran outrigger layout based on NSGA-II[J]. *Applied Ocean Research*, 2018, 78: 110-122.

Zheng L, Liu Z, Yang S, et al. Optimal design and installation of appendages for improving stability performance of a trimaran[J]. *Ocean Engineering*, 2021, 238: 109719.

Zeng B, Song Y, Zheng L. A method of a trimaran vertical movements reduction control and hardware realization [J]. *IEEE Access*, 2019, 7: 102209-102216.